

# Supercapacitor Electrodes with High-Energy and Power Densities Prepared from Monolithic NiO/Ni Nanocomposites\*\*

Qi Lu, Michael W. Lattanzi, Yunpeng Chen, Xiaoming Kou, Wanfeng Li, Xin Fan, Karl M. Unruh, Jingguang G. Chen, and John Q. Xiao\*

The depletion of traditional energy resources as well as the desire to reduce high CO<sub>2</sub> emissions associated with their use has led to significant interest in developing sustainable and clean energy products,<sup>[1–4]</sup> such as electricity produced from wind- or solar-based technologies. Because of the intermittent availability of these resources the realization of their full potential will also require the development of new and advanced energy-storage and delivery systems. Supercapacitors, as a new class of energy storage devices, are now attracting intensive attention<sup>[2]</sup> because of their ability to store energy comparable to certain types of batteries, but with the advantage of delivering the stored energy much more rapidly than batteries.<sup>[3]</sup> This property makes supercapacitor ideal to augment traditional batteries in many different applications. However, to become primary devices for power supply, supercapacitors must be developed further to improve their abilities to deliver, simultaneously, high energy and power.<sup>[5]</sup>

To realize this objective, nanostructured electrodes have been developed from a variety of different functional materials.<sup>[6–10]</sup> Despite significant progress, however, most of the processes for the fabrication of electrodes are either too delicate,<sup>[11–14]</sup> which makes them less viable for large-scale industrial applications, or require additives,<sup>[15,16]</sup> which deteriorates the performance of the electrodes. In addition, previously reported electrode materials with the desirable specific capacitance typically show high resistances,<sup>[9,13,17]</sup> which not only restrict the power performance but also prevent the utilization of thick electrodes. Based on these considerations, the goal of the present work was to build an advanced supercapacitor electrode using a simple and scalable fabrication technique and to optimize the electrode performance using a controlled functional material and a well-defined electrode network with minimum resistivity. First, Ni nanoparticles were synthesized using a modified polyol process.<sup>[18]</sup> After a simple mechanical compaction of the as-prepared (AP) nanoparticles and a subsequent low-temperature annealing process, monolithic and mechanically robust, stable, and low-resistivity NiO/Ni nanoporous com-

posite electrodes were obtained with both maximized energy and power densities.

The structure of the AP Ni particles was characterized by X-ray diffraction (XRD; Figure 1 a) and electron diffraction (ED; Figure 1 b). The particle size estimated from the Scherrer method was 4.4 nm, and several particles formed larger aggregates with a diameter smaller than 20 nm (Figure 1 b); these findings are in agreement with the measured

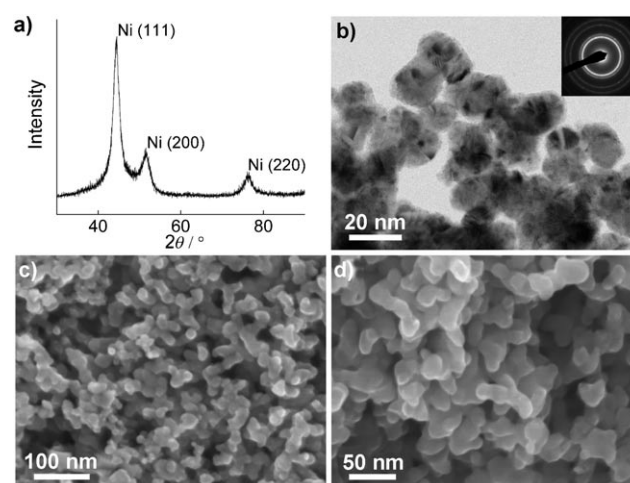


**Figure 1.** Characterization of the structure: a) XRD pattern of the as-prepared Ni nanoparticles. b) Transmission electron microscopic (TEM) image and ED pattern of the as-prepared Ni nanoparticles. Scanning electron microscopic images at the c) surface and d) cross-section of prototype electrodes.

Brunauer–Emmett–Teller (BET) surface area of 40 m<sup>2</sup> g<sup>-1</sup>. The AP particles were then mechanically compacted into monolithic pellets and used as prototype electrodes. These pellets are stable, easy to handle, and did neither require additives nor a supporting substrate. Scanning electron microscopic images obtained at both the surface and cross-section (Figure 1 c,d) of these electrodes revealed a highly porous structure formed by a network of Ni nanoparticles. BET measurements of these pellets (ca. 37 m<sup>2</sup> g<sup>-1</sup>) suggested that most of the surface area of the nanoparticles was not affected by the preparation technique.

After sputter deposition of an 80 nm thick Pt layer on one side of the pellets which serves as a current collector, we performed a thermal annealing process (in atmospheric air) to create NiO shells around the pellets that are the active layer in their application as supercapacitors. Figure 2 shows

[\*] Q. Lu, M. W. Lattanzi, Y. Chen, Dr. X. Kou, Dr. W. Li, Dr. X. Fan, Prof. Dr. K. M. Unruh, Prof. Dr. J. Q. Xiao  
 Department of Physics and Astronomy  
 University of Delaware, Newark, DE 19716 (USA)  
 Fax: (+1) 302-831-1637  
 E-mail: jqx@udel.edu

Prof. Dr. J. G. Chen  
 Department of Chemical Engineering, University of Delaware (USA)

[\*\*] We acknowledge financial support from the Office of Naval Research under grant number N00014-08-1-0432.

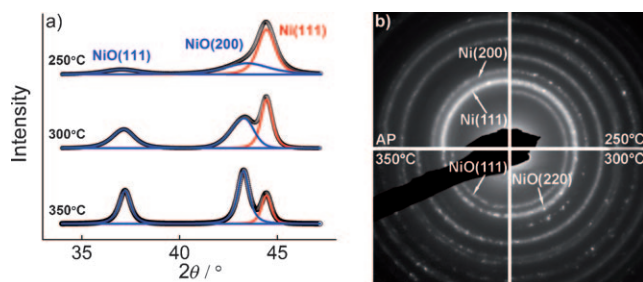


**Figure 2.** Characterization of the oxidation process: a) XRD patterns and b) ED patterns of the NiO/Ni nanoparticles oxidized at different temperatures.

the XRD and ED patterns of the NiO/Ni nanocomposites oxidized at different temperatures. At 250°C the appearance of broad peaks at diffraction angles of about 37 and 43° displays the presence of a NiO phase consisting of very small crystallites. At higher annealing temperatures these peaks decreased in width and increased in intensity. Similar results were also observed in the corresponding ED pattern. Vibrating sample magnetometer (VSM) measurements were also performed on the samples to determine the saturation magnetizations. The ratio of Ni to NiO was determined by comparing the magnetization loss of the annealed and the AP samples and used to calculate the specific capacitance of the samples.

Working electrodes were fabricated for electrochemical characterization by attaching Pt wires to the Pt-coated annealed pellets. An aqueous 1M KOH solution was chosen as electrolyte because NiO is stable in this solution. Figure 3a,b shows the cyclic voltammograms and cyclic chronopotentiometric plots of the electrodes prepared at different annealing temperatures. The peaks of the redox currents in Figure 3a and the transition periods of the potentials in

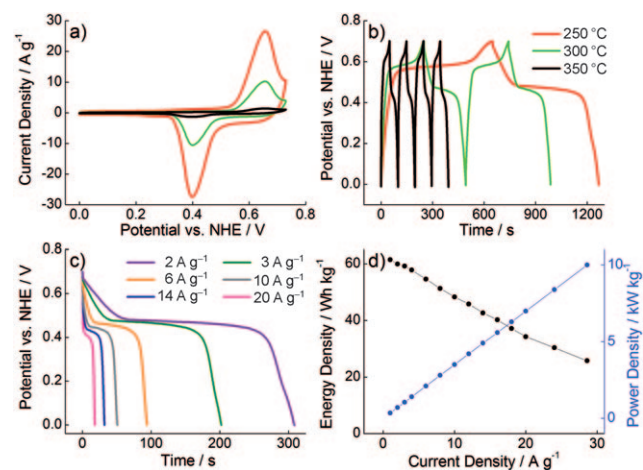


**Figure 3.** Electrochemical characterization: a) Cyclic voltammograms at a scan rate of 5 mVs<sup>-1</sup> and b) cyclic chronopotentiometric curves with a charge/discharge current density of 1 A g<sup>-1</sup> for the electrodes prepared at different temperatures. c) Cyclic chronopotentiometric curves of a sample at 250°C for various charge/discharge currents and d) accordingly derived energy and power densities.

Figure 3b display the reversible process of insertion and extraction of OH<sup>-</sup> anions according to Equation (1)



The electrodes oxidized at 250°C show a significantly better performance than their high-temperature counterparts. The average specific capacitance (SC) was calculated to be 910 F g<sup>-1</sup> from cyclic voltammetry (CV) and 905 F g<sup>-1</sup> from cyclic chronopotentiometry (CC) based on the mass of NiO (ca. 300 F g<sup>-1</sup> based on the total electrode mass), and the SC drops to 348 F g<sup>-1</sup> at 300°C and further to 72 F g<sup>-1</sup> at 350°C. The SC performance of the sample annealed at 250°C is remarkable for two reasons: first, the high density of the grain boundaries as a result of the very small particle size of the NiO shell creates efficient diffusion paths for the OH<sup>-</sup> ions, which significantly enhances the intercalation of the electrolyte ions and, therefore, the utilization of the electrode material.<sup>[19,20]</sup> Second, the conductive network of metal cores is well-maintained since the oxide shell is estimated to be about 3 nm. More intense oxidation at higher temperatures tends to isolate the conductive cores and gives rise to a much higher ohmic resistivity of the electrode as shown in Figure 4a. The ohmic resistivity of the electrode reduces the

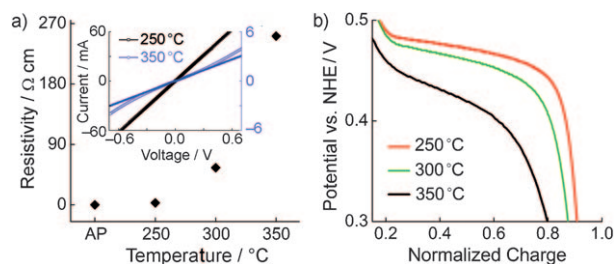


**Figure 4.** Characterization of the conductivity: a) Resistivities of samples prepared at different thermal conditions. Inset: *I*-*V* curves and associated linear fits within the range of -0.1 to 0.1 V. At 250°C the sample behaves like a metal, whereas at 350°C it shows a tunneling effect because of the isolated conductive metal cores. b) Reconstructed cyclic chronopotentiometric curves of discharge (measured at 1 A g<sup>-1</sup>) with respect to the normalized charge. At each potential of discharge, electrodes with the lowest ohmic resistivity show the highest utilization of the electrode material (NHE = normal hydrogen electrode).

utilization of the electrode material because of polarization loss.<sup>[21,22]</sup> This phenomenon can be observed by reconstructing the cyclic chronopotentiometric curves from the electrode potential and the normalized charge (stored/released charge scaled to the total capacity). The utilization of the electrode material can thus be qualitatively compared at each potential of the electrode (Figure 4b). High utilization of the electrode is observed for a sample oxidized at low temperature, indicating that the electrode performance is enhanced by a small ohmic resistivity originating from the conductive network of metal cores. Another advantage of the conductive network of metal cores is that the resistivity of the electrode does not depend on the size of the electrode itself, which facilitates its commercial production at large scale.

The most important advantage of supercapacitors is their much higher power density relative to that of ordinary batteries. Therefore, the high-power performance of the electrodes was characterized by a series of cyclic chronopotentiometric measurements with charge/discharge current densities up to  $28.6 \text{ A g}^{-1}$  (equivalent to  $10 \text{ kW kg}^{-1}$  of power density; Figure 3c). The reversible redox reaction between NiO and  $\text{OH}^-$  [Eq. (1)], is a highly diffusion-controlled process.<sup>[23]</sup> Therefore, it can be expected that the SC, and thus the obtained energy density, will decrease at fast charge/discharge rate. This phenomenon has been observed in most of the previous studies.<sup>[24–27]</sup> In Figure 3d the energy density as well as the power density is plotted versus the current density. At a slow charge/discharge rate ( $1 \text{ A g}^{-1}$ ) a high-energy density of  $62 \text{ Wh kg}^{-1}$  (equivalent to  $905 \text{ F g}^{-1}$  for the SC) was observed. However, the power density achieved at this rate (ca.  $0.4 \text{ kW kg}^{-1}$ ) was small relative to that of electrochemical double-layer capacitors (EDLCs) which show a fast mechanism for the storage of surface charges.<sup>[18,28,29]</sup> As the charge/discharge rate was increased to  $28.6 \text{ A g}^{-1}$ , a high-power density of  $10 \text{ kW kg}^{-1}$  was achieved. Although the corresponding energy density dropped to  $26 \text{ Wh kg}^{-1}$  (equivalent to  $380 \text{ F g}^{-1}$  for the SC), it still is one of best performances reported so far.<sup>[3]</sup>

In most applications that require an energy storage system the process of energy collection is usually slow (e.g., wind or solar-power plant), but the stored energy must be released rapidly to meet the power demands of these applications. Therefore, the NiO/Ni nanocomposite electrodes were first charged at a small current density ( $1 \text{ A g}^{-1}$ ) and then discharged at a series of higher discharge rates (Figure 5a). The power densities of discharge, average specific capacitances of discharge, and calculated energy densities of discharge were obtained from the discharge portion of the cyclic chronopotentiometric curves. As shown in Figure 5b, the energy density of discharge is only slightly affected by the discharge rates. Outstanding performances of high-energy (ca.  $60 \text{ Wh kg}^{-1}$ ) and high-power densities ( $10 \text{ kW kg}^{-1}$ ) were simultaneously achieved.

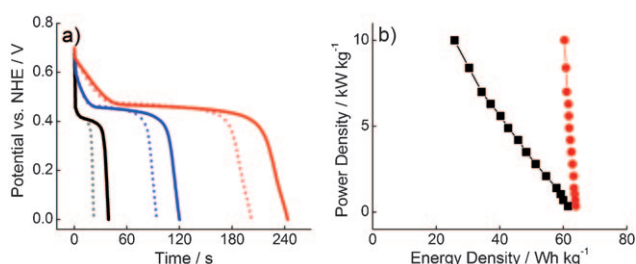


**Figure 5.** Slow-charge and fast-discharge characterization. a) Cyclic chronopotentiometric curves with a density of charge currents of  $1 \text{ A g}^{-1}$  and various densities of discharge currents (ratio of the charge to the discharge current density: solid lines in red  $1/3 \text{ A g}^{-1}$ , in blue  $1/6 \text{ A g}^{-1}$ , and in black  $1/18 \text{ A g}^{-1}$ ; dotted lines in red  $3/3 \text{ A g}^{-1}$ , in blue  $6/6 \text{ A g}^{-1}$ , and in gray  $18/18 \text{ A g}^{-1}$ ). b) Ragon plot (power density vs. energy density) derived from the discharge portion of the cyclic chronopotentiometric curves (● charge with  $1 \text{ A g}^{-1}$ ; ■ ratio of the charge to the discharge current density with the same current density).

In summary, the current study reports a simple, cost-effective, and potentially scalable technique for fabricating monolithic NiO/Ni nanocomposite electrodes for electrochemical supercapacitors. The electrodes annealed at  $250^\circ\text{C}$  showed a remarkably high specific capacitance (ca.  $900 \text{ F g}^{-1}$ ) because of the highly activated NiO surface layer and the conductive network of metal cores. High-energy (ca.  $60 \text{ Wh kg}^{-1}$ ) and high-power ( $10 \text{ kW kg}^{-1}$ ) densities were achieved with slow and fast charge/discharge rates, respectively. For longer times of energy storage, the delivery of energy density was not affected by the output power.

### Experimental Section

The Ni nanoparticles were synthesized by a modified polyol process. Solid  $\text{NiCl}_2 \cdot 6\text{H}_2\text{O}$  (Alfa Aesar, 1.0 g) was dissolved in ethylene glycol (Alfa Aesar, 250 mL) at room temperature by mechanical stirring. The solution was then heated to reflux at  $(195 \pm 2)^\circ\text{C}$ . Once a stable temperature had been reached, solid  $\text{NaBH}_4$  (Strem Chemicals, 2.0 g) was added to the solution as a reducing agent. The mixture was subsequently maintained at reflux for 30 min and then cooled to room temperature. The resulting particles were magnetically isolated, repeatedly washed in a sonicated bath with acetone and ethyl alcohol, and then dried in vacuum at  $100^\circ\text{C}$  overnight.

Electrodes for the characterization of the supercapacitor were prepared by mechanically compacting a specified mass (5 mg) of Ni powder in a hydraulic press to produce thin pellet disks of 4 mm indiameter. A Pt layer (80 nm) was then splutter coated on one side of the pellet to serve as the current collector. The electrodes were thermally annealed in air at different temperatures (for 1 hour) to create a NiO shell with supercapacitance.

The electrochemical measurements were carried out in a beakertype electrochemical half-cell setup equipped with an Ag/AgCl (saturated KCl) reference electrode (Fisher Scientific) and a platinum-plate counterelectrode. A KOH solution (1M) was used as electrolyte. The working electrode was impregnated with the electrolyte for 30 min to ensure that the NiO/Ni nanocomposite electrode was thoroughly wet. Cyclic voltammetry and cyclic chronopotentiometric measurements were performed on a potentiostat/galvanostat (PRA 263A) to determine the electrochemical properties. Average specific capacitance values determined from the cyclic voltammometric curves were calculated according to Equation (2),

$$C = \frac{\int Idt}{m\Delta V} \quad (2)$$

where  $I$  is the oxidation/reduction current,  $dt$  is the time differential,  $m$  is the mass of the active electrode material, and  $\Delta V$  is the voltage range of one scanning segment. The specific capacitance, energy density ( $d_e$ ), and power density ( $d_p$ ) were also calculated from the cyclic chronopotentiometric curves according to Equations (3–5),

$$C = \frac{I\Delta t}{m\Delta V} \quad (3)$$

$$d_e = \frac{1}{2}C(\Delta V)^2 \quad (4)$$

$$d_p = \frac{d_e}{\Delta t} \quad (5)$$

where  $I$  is the charge/discharge current,  $\Delta t$  is the time for a full charge or discharge,  $m$  is the mass of the active material, and  $\Delta V$  is the voltage change after a full charge or discharge.

Received: February 13, 2011  
 Published online: May 30, 2011

**Keywords:** electrochemistry · metal oxides · nanoparticles · supercapacitors

- 
- [1] A. S. Aricò, P. Bruce, B. Scrosati, J. M. Tarascon, W. Van Schalkwijk, *Nat. Mater.* **2005**, *4*, 366.
- [2] C. Liu, F. Li, L. P. Ma, H. M. Cheng, *Adv. Mater.* **2010**, *22*, E28.
- [3] P. Simon, Y. Gogotsi, *Nat. Mater.* **2008**, *7*, 845.
- [4] D. V. Esposito, S. T. Hunt, A. L. Stottlemyer, K. D. Dobson, B. E. McCandless, R. W. Birkmire, J. G. Chen, *Angew. Chem.* **2010**, *122*, 10055; *Angew. Chem. Int. Ed.* **2010**, *49*, 9859.
- [5] A. Burke, *J. Power Sources* **2000**, *91*, 37.
- [6] J. Bae, M. K. Song, Y. J. Park, J. M. Kim, M. Liu, Z. L. Wang, *Angew. Chem.* **2011**, *123*, 1721; *Angew. Chem. Int. Ed.* **2011**, *50*, 1683.
- [7] K. Brezesinski, J. Wang, J. Haetge, C. Reitz, S. O. Steinmueller, S. H. Tolbert, B. M. Smarsly, B. Dunn, T. Brezesinski, *J. Am. Chem. Soc.* **2010**, *132*, 6982.
- [8] D. N. Futaba, K. Hata, T. Yamada, T. Hiraoka, Y. Hayamizu, Y. Kakudate, O. Tanaike, H. Hatori, M. Yumura, S. Iijima, *Nat. Mater.* **2006**, *5*, 987.
- [9] W. Sugimoto, H. Iwata, Y. Yasunaga, Y. Murakami, Y. Takasu, *Angew. Chem.* **2003**, *115*, 4226; *Angew. Chem. Int. Ed.* **2003**, *42*, 4092.
- [10] X. L. Wu, L. Y. Jiang, F. F. Cao, Y. G. Guo, L. J. Wan, *Adv. Mater.* **2009**, *21*, 2710.
- [11] Y. Y. Liang, M. G. Schwab, L. J. Zhi, E. Mugnaioli, U. Kolb, X. L. Feng, K. Mullen, *J. Am. Chem. Soc.* **2010**, *132*, 15030.
- [12] T. Brezesinski, J. Wang, S. H. Tolbert, B. Dunn, *Nat. Mater.* **2010**, *9*, 146.
- [13] H. L. Wang, H. S. Casalongue, Y. Y. Liang, H. J. Dai, *J. Am. Chem. Soc.* **2010**, *132*, 7472.
- [14] J. S. Ye, H. F. Cui, X. Liu, T. M. Lim, W. D. Zhang, F. S. Sheu, *Small* **2005**, *1*, 560.
- [15] V. Subramanian, H. W. Zhu, R. Vajtai, P. M. Ajayan, B. Q. Wei, *J. Phys. Chem. B* **2005**, *109*, 20207.
- [16] K. H. An, W. S. Kim, Y. S. Park, J. M. Moon, D. J. Bae, S. C. Lim, Y. S. Lee, Y. H. Lee, *Adv. Funct. Mater.* **2001**, *11*, 387.
- [17] Q. T. Qu, P. Zhang, B. Wang, Y. H. Chen, S. Tian, Y. P. Wu, R. Holze, *J. Phys. Chem. C* **2009**, *113*, 14020.
- [18] F. Fievet, J. P. Lagier, B. Blin, B. Beaudoin, M. Figlarz, *Solid State Ionics* **1989**, *32–3*, 198.
- [19] J. P. Zheng, T. R. Jow, *J. Electrochem. Soc.* **1995**, *142*, L6.
- [20] Y. Abe, S. H. Lee, E. O. Zayim, C. E. Tracy, J. R. Pitts, S. K. Deb, *Jpn. J. Appl. Phys. Part 1* **2006**, *45*, 7780.
- [21] J. W. Weidner, P. Timmerman, *J. Electrochem. Soc.* **1994**, *141*, 346.
- [22] O. Lanzi, U. Landau, *J. Electrochem. Soc.* **1991**, *138*, 2527.
- [23] P. C. Yu, G. Nazri, C. M. Lampert, *Sol. Energy Mater.* **1987**, *16*, 1.
- [24] K. R. Prasad, N. Miura, *Appl. Phys. Lett.* **2004**, *85*, 4199.
- [25] T. Brezesinski, J. Wang, J. Polleux, B. Dunn, S. H. Tolbert, *J. Am. Chem. Soc.* **2009**, *131*, 1802.
- [26] J. P. Zheng, T. R. Jow, *J. Power Sources* **1996**, *62*, 155.
- [27] Q. Lu, Z. J. Mellinger, W. Wang, W. Li, Y. Chen, J. G. Chen, J. Q. Xiao, *ChemSusChem* **2010**, *3*, 1367.
- [28] J. Liu, G. Z. Cao, Z. G. Yang, D. H. Wang, D. Dubois, X. D. Zhou, G. L. Graff, L. R. Pederson, J. G. Zhang, *ChemSusChem* **2008**, *1*, 676.
- [29] D. S. Su, R. Schlögl, *ChemSusChem* **2010**, *3*, 136.
-